Astron. Astrophys. 326, 396–411 (1997)

ASTRONOMY
AND
ASTROPHYSICS

Variation of bulk velocity and temperature anisotropy of neutral heliospheric hydrogen during the solar cycle

Maciej Bzowski[1], **Hans J. Fahr**[2], **Daniel Ruciński**[1], **and Horst Scherer**[2]

[1] Space Research Centre of the Polish Academy of Sciences, Bartycka 18 A, PL-00-716 Warsaw, Poland
[2] Institut für Astrophysik und Extraterrestrische Forschung der Universität Bonn, Auf dem Hügel 71, D-53121 Bonn, Germany

Received 6 January 1997 / Accepted 24 April 1997

Abstract. Using a time-dependent kinetic approach the density, bulk velocity vector, and temperature tensor of interstellar hydrogen in the inner Solar System in several phases of solar cycle were computed. Model solar cycle time-profiles of hydrogen ionisation rate and Lyman-α radiation pressure were used, solar latiudinal effects and filtration at the heliospheric interface were neglected. It was concluded that due to the joint action of solar ionisation and radiation pressure the bulk velocity of the gas is strongly variable during solar cycle and, within 15–30 AU from the Sun, it significantly changes with the heliocentric distance both in magnituide and direction. The changes typically are about 15 km/s and exceed the thermal spread of the gas. The temperature is strongly anisotropic; the anisotropy is strongly variable in time and it fades off with the heliocentric distance. The projections of temperature tensor on various lines can change from 5 000 to 11 000 K upwind and from $\sim$ 12 000 to 45 000 K downwind at 1 AU and from 6 000 to 8 000 K upwind and from 8 000 to 15 000 K downwind at 10 AU. For optical observations an important quantity is the radial temperature. For lines of sight directed radially away from the Sun the change of radial temperature along the sightline is strongest during solar minimum and it is equal to about 3 000 K in the upwind direction and to about 5 000 K in the downwind direction. The smallest change occurs during solar maximum. The upwind-to-downwind ratio of intensity of backscattered radiation varies during the solar cycle by about 20% around the mean value. A brief discussion of theoretical spectra of interplanetary lines is provided. The main conclusion is that for observations carried out from 1 AU the Doppler shift of interplanetary lines corresponds to the bulk speed "in infinity" for the lines of sight directed downwind; for the lines of sight directed upwind the Doppler shift corresponds to the bulk speed increased by about 25% in comparison with the bulk speed "in infinity" except solar maximum epoch, when the increase is only 1 to 2 km/s. The width of interplanetary lines returns the temperature of the gas "in infinity" only for the lines of sight directed upwind; for the lines of sight directed crosswind and downwind the line width returns temperatures higher by about 3 000 K and no simple seasonal correlation can be observed.

Key words: solar system: interplanetary medium – Sun: activity

1. Introduction

The problem of neutral gas species of the Local Interstellar Medium (LISM) entering the heliospheric plasma regime and subjected to numerous solar-induced ionising and radiative processes has been studied for several decades. Clearly, in view of the relevant mean free paths for elastic atom–atom collisions, the appropriate method to theoretically describe this scenario is the kinetic theory on the basis of the Boltzmann integro-differential equation which meanwhile has been applied in different forms to this problem (e.g. Fahr 1971, 1978; Holzer 1977; Wu & Judge 1979; Thomas 1978; Fahr 1979). In more recent years, also the modulating effect of perturbed plasma flows in the heliospheric and interstellar plasma interface has been studied (Ripken & Fahr 1983; Fahr & Ripken 1984; Fahr 1986, 1991; Osterbart & Fahr 1992; Fahr et al. 1993; Zank et al. 1996; Williams et al. 1996; Pauls et al. 1995, 1996; Zank & Pauls 1996). In the paper by Baranov & Malama (1993) the interface effect on neutral LISM gases has been described by the use of Monte Carlo calculations. On the other hand, several attempts to model the influence of time-variability of solar cycle-related phenomena on the distribution of neutral hydrogen within the Solar System have been undertaken (e.g. Kyrölä et al. 1994; Bzowski & Ruciński 1995a,b; Ruciński & Bzowski 1995; Summanen 1996). Modelling efforts were recently reviewed by Ruciński & Bzowski (1996). It was demonstrated that the solar variabilities significantly influence the density distribution within several astronomical units around the Sun and may have consequences reflected in current experimental data.

In this paper higher moments of the neutral hydrogen distribution function, namely the bulk velocity vector and temperature tensor, are studied. We start with a brief discussion of the

Send offprint requests to: M. Bzowski

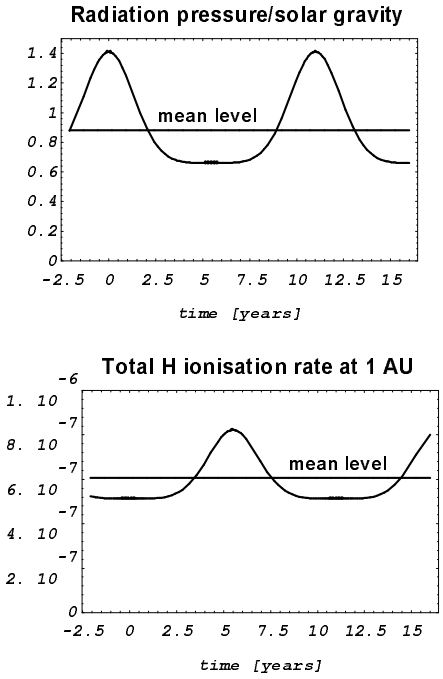

Fig. 1. The course of solar radiation pressure expressed in the units of solar gravity (upper panel) and total ionisation rate for hydrogen at 1 AU (lower panel) during the solar cycle, as adopted in this paper. Time equal 0 corresponds to the solar maximum epoch. Note the anticorrelation of the two functions.

model used, we provide the formulae to compute the moments of distribution function and we briefly review the results on the variability of neutral hydrogen density. In the following section we discuss the bulk velocity and temperature tensor of the gas both in the static and time-dependent approaches. At the end we consider some examples of the effect of variations of velocity and temperature within the Solar System on the intensities and line profiles of the backscattered Lyman-α radiation.

2. Basic model assumptions

It is assumed that the interstellar neutral hydrogen gas surrounding the heliosphere (i.e. "at infinity", as it will be referred to in the paper) is homogeneous and that it flows into the Solar System with a bulk velocity $v_{\rm B}$ without interaction with the heliospheric interface. The gas "at infinity" has a temperature T_0 and density n_0. The atoms are subjected to a spherically symmetric force of solar gravity and solar Lyman-α radiation pressure modelled as a continuous, non-stochastic phenomenon, however variable in time. The gravity and radiation pressure produce a time dependent net force depending on the heliocentric distance r like $1/r^2$. The atoms following their trajectories within the Solar System are subjected to various ionising processes. These processes are also variable in time but generally their intensity falls off like $1/r^2$, too. They include the resonant charge exchange with solar wind protons, photoionisation from the solar radiative output, and collisional ionisation with electrons. This latter process is significant only well inside 1 AU around the Sun; because its influence on the overall picture is minor, it will be disregarded.

It is further assumed that variations of all ionising and radiative processes occur instantaneously throughout the Solar System. This means that the retardation of the solar wind-related variabilities, resulting from finite distances to the Sun and a finite speed of propagation, are neglected. In view of the typical solar wind speed of the order of 500 km/s, this brings an evident lower limitation to the time scale of variations to longer than about 1 year. Details of the assumptions and the discussion of the computational method used can be found in Ruciński & Bzowski (1995).

The parameters of neutral gas in the interstellar surroundings of the heliosphere are not precisely known. Recent astrophysical studies of the lines of sight towards nearby stars permit to conclude that the Sun is immersed in a small cloud with the temperature around 6000 K that travels relative to the Sun at about 26 km/s (e.g. Lallement, 1996); this result agrees with direct determination of kinematic parameters of interstellar gas from in situ helium measurements on Ulysses (Witte et al., 1996).

The presented model is simplistic in this respect that it takes into account only the time variability during the solar cycle but it does not include the influence of the heliospheric interface on the parameters of the gas. However, one cannot neglect the interface influence altogether. From the papers published so far (see recent reviews by Lallement (1996) and Fahr (1996)) one can infer that the heliospheric interface does some filtering, heating and slowing down of the interstellar hydrogen gas at larger distances from the Sun, whereas at smaller distances mainly solar imprints are contributing. The influence of the interface on the local distribution function of the gas and its moments depends on the angular distance off the upwind direction and the heliocentric distance. At the wind axis at 50 AU from the Sun the filtered neutral gas has a bulk velocity of about 20 km/s and a temperature of about 8000 K. Its density is probably reduced roughly by half in comparison with the unperturbed density in the Very Local Interstellar Medium (VLISM) but this quantity anyway is known with poorest accuracy. Since the interface models predict an extended density plateau around 50 AU, the density at 50 AU and the gas velocity decelerated to 20 km/s can be taken as initial values in our model.

For the purposes of this modelling it is assumed that the gas "at infinity" flows with the bulk velocity of 20 km/s, has the temperature of 8000 K and density of 0.1 cm^{-3}. It is worth to note that the theory presented further in most applications is linear in density.

The adopted courses of radiation pressure and ionisation rate during solar cycle are presented in Fig. 1. They are model approximations of the physical reality, reflecting the range of variations of the relevant quantities, the correlation of radiation pressure with solar activity and the anticorrelation of charge exchange ionisation rate. However, these model representations do not pretend to reflect exactly the variabilities as measured by various spacecraft.

The model variabilities presented above form the basis for a stationary model called the MSM (Mean Stationary Model),

which will serve as a reference for the variabilities investigated in this paper. This model is the classical "hot" model in the formulation by Wu & Judge (1979). The parameters of the MSM model are the following: temperature "at infinity" $T = 8000$ K, bulk velocity "at infinity" (typically 50 AU) $v_B = 20$ km/s, and $\mu = 0.89$, $\beta_0 = 6.06 \cdot 10^{-7}\mathrm{s}^{-1}$; the two latter quantities are the mean values of $\mu(t)$ and $\beta(t)$ over the solar cycle.

3. Computation of moments of the hydrogen distribution function

The problem of computation of time-variable hydrogen density within the heliosphere has been extensively discussed by Ruciński & Bzowski (1995). Further on in this article we present a brief recapitulation and the formulae for higher moments of hydrogen distribution functions as used in this study.

The problem has axial symmetry with the symmetry axis corresponding to the direction of inflow of the interstellar matter. The reference system is defined as follows. Let us take the heliocentric distance of a selected location within the Solar System as r and its polar angle θ with respect to the inflow axis. The selected plane must contain the Sun and the inflow axis and is inclined to the ecliptic by an arbitrary but fixed angle ψ. The plane specified in this way will be referred to throughout the paper as *the reference plane*. Thanks to the axial symmetry of the problem one needs to compute the moments of the distribution function in the selected reference plane only, thus getting rid of the dependence on the second space angle. From now on we thus restrict ourselves to locations in the reference plane.

As velocity components we select the radial velocity v_r, the transversal velocity v_ρ and the angle κ of inclination of atomic orbital plane to the reference plane. The angle κ varies from 0 to 2π, the radial velocity v_r from minus to plus infinity, and the transversal velocity v_ρ from 0 to infinity. The distribution function of hydrogen atoms in the reference plane is thus defined to depend on the following variables:

$$f_H = f_H(r, \theta, v_r, v_\rho, \kappa, t) \tag{1}$$

The density in the reference plane is computed from the formula

$$\begin{aligned} n_H(r,\theta,t) &= \iiint_v f_H(r,\theta,v_r,v_\rho,\kappa,t)\,\mathrm{d}^3v = \\ &= \int_{-\infty}^{\infty}\int_0^{\infty}\int_0^{2\pi} f_H(r,\theta,v_r,v_\rho,\kappa,t)\,\mathrm{d}\kappa\, v_\rho\,\mathrm{d}v_\rho\,\mathrm{d}v_r \end{aligned} \tag{2}$$

and the higher moments $\langle P\rangle$ from the formula

$$\begin{aligned} \langle P\rangle(r,\theta,t) &= \\ &= \frac{\int_{-\infty}^{\infty}\int_0^{\infty}\int_0^{2\pi} P\, f_H(r,\theta,v_r,v_\rho,\kappa,t)\,\mathrm{d}\kappa\, v_\rho\,\mathrm{d}v_\rho\,\mathrm{d}v_r}{n_H(r,\theta,t)} \\ &= \int_{-\infty}^{\infty}\int_0^{\infty}\int_0^{2\pi} P\,\tilde{f}_H(r,\theta,v_r,v_\rho,\kappa,t)\,\mathrm{d}\kappa\, v_\rho\,\mathrm{d}v_\rho\,\mathrm{d}v_r \end{aligned} \tag{3}$$

where $\tilde{f}$ is the normalised distribution function, i.e.

$$\int_{-\infty}^{\infty}\int_0^{\infty}\int_0^{2\pi} \tilde{f}_H\,\mathrm{d}\kappa\, v_\rho\,\mathrm{d}v_\rho\,\mathrm{d}v_r = \int_{-\infty}^{\infty}\int_0^{\infty}\int_0^{2\pi} \frac{f_H}{n_H}\,\mathrm{d}\kappa\, v_\rho\,\mathrm{d}v_\rho\,\mathrm{d}v_r = 1 \tag{4}$$

and $\langle P\rangle$ and P stand for the following quantities:

$\langle v_r\rangle$	v_r
$\langle v_{\rho,1}\rangle$	$v_\rho \cos\kappa$
$\langle v_{\rho,2}\rangle$	$v_\rho \sin\kappa$
$\langle v_r^2\rangle$	v_r^2
$\langle v_{\rho,1}^2\rangle$	$(v_\rho\cos\kappa)^2$
$\langle v_{\rho,2}^2\rangle$	$(v_\rho\sin\kappa)^2$
$\langle v_r v_{\rho,1}\rangle$	$v_r v_\rho \cos\kappa$
$\langle v_r v_{\rho,2}\rangle$	$v_r v_\rho \sin\kappa$
$\langle v_{\rho,1} v_{\rho,2}\rangle$	$v_\rho^2 \sin\kappa\cos\kappa$

It can be proved (see Ruciński & Bzowski 1995) that the distribution function can be expressed in the form:

$$\begin{aligned} f_H(r,\theta,\kappa,v_r,v_\rho,t) &= h(r,\theta,v_r,v_\rho,t)\times \\ &\times \exp\left[g(r,\theta,v_r,v_\rho,t)\cos\kappa\right] \end{aligned} \tag{5}$$

where h and g are appropriate functions independent of κ, and thanks to the axial symmetry the integration over κ can be immediately performed analytically using an appropriate modified Bessel function. Then the resulting formulae become as follows:

$$n_H = 2\pi \int_{-\infty}^{\infty}\int_0^{\infty} v_\rho\,\mathrm{d}v_\rho\,\mathrm{d}v_r\; hI_0(g) \tag{6}$$

$$\langle v_r\rangle = \frac{2\pi}{n_H}\int_{-\infty}^{\infty}\int_0^{\infty} v_\rho\,\mathrm{d}v_\rho\,\mathrm{d}v_r\; v_r h I_0(g) \tag{7}$$

$$\langle v_{\rho,1}\rangle = \frac{2\pi}{n_H}\int_{-\infty}^{\infty}\int_0^{\infty} v_\rho\,\mathrm{d}v_\rho\,\mathrm{d}v_r\; v_\rho h I_1(g) \tag{8}$$

$$\langle v_{\rho,2}\rangle = 0 \tag{9}$$

$$\langle v_r^2\rangle = \frac{2\pi}{n_H}\int_{-\infty}^{\infty}\int_0^{\infty} v_\rho\,\mathrm{d}v_\rho\,\mathrm{d}v_r\; v_r^2 h I_0(g) \tag{10}$$

$$\langle v_{\rho,1}^2\rangle = \frac{2\pi}{n_H}\int_{-\infty}^{\infty}\int_0^{\infty} v_\rho\,\mathrm{d}v_\rho\,\mathrm{d}v_r\; v_\rho^2 h \frac{I_1(g)}{g} \tag{11}$$

$$\langle v_{\rho,2}^2\rangle = \frac{2\pi}{n_H}\int_{-\infty}^{\infty}\int_0^{\infty} v_\rho\,\mathrm{d}v_\rho\,\mathrm{d}v_r\; v_\rho^2 h \left(I_0(g) - \frac{I_1(g)}{g}\right) \tag{12}$$

$$\langle v_r v_{\rho,1}\rangle = \frac{2\pi}{n_H}\int_{-\infty}^{\infty}\int_0^{\infty} v_\rho\,\mathrm{d}v_\rho\,\mathrm{d}v_r\; v_r v_\rho h I_1(g) \tag{13}$$

$$\langle v_r v_{\rho,2} \rangle = 0 \tag{14}$$

$$\langle v_{\rho,1} v_{\rho,2} \rangle = 0 \tag{15}$$

In these formulae $I_0(g)$ and $I_1(g)$ are the modified Bessel functions of the first kind and, respectively, of 0-th and 1-st order. The moment $\langle v_{\rho,1} \rangle$ is the component of bulk velocity perpendicular to the local radius vector, laying in the reference plane, while $\langle v_{\rho,2} \rangle$ is the bulk velocity component perpendicular to both $\langle v_{\rho,1} \rangle$ and $\langle v_r \rangle$. As one should expect, $\langle v_{\rho,2} \rangle$ is equal to zero because there is no spiral motion of the bulk flow of the gas. However, one does expect a thermal spread in velocities along all three cardinal directions, and sure enough, none of the $\langle v_i^2 \rangle$ moments disappears.

The local bulk velocity vector of the gas in the reference plane is defined by the formula:

$$\boldsymbol{v}_{\mathrm{B}} = \iiint\limits_{v} \boldsymbol{v} \tilde{f}_{\mathrm{H}} \, \mathrm{d}^3 v = \left[\langle v_r \rangle, \langle v_{\rho,1} \rangle, \langle v_{\rho,2} \rangle = 0 \right], \tag{16}$$

where the coordinates are defined in Eqs. (7,8,9), and its projection on a direction inclined at an angle α to the radius-vector in the reference plane is given by the formula

$$\langle v_\alpha \rangle = \langle v_r \rangle \cos\alpha + \langle v_{\rho,1} \rangle \sin\alpha. \tag{17}$$

A measure of thermal spread along a selected direction is the local kinetic temperature, defined as follows:

$$T_\alpha = \frac{m_{\mathrm{H}}}{k} \iiint\limits_{v} \left(v_\alpha - \langle v_\alpha \rangle \right)^2 \tilde{f}_{\mathrm{H}} \, \mathrm{d}^3 v \tag{18}$$

which evaluates to the form

$$T_\alpha = \frac{m_{\mathrm{H}}}{k} \left(\langle v_\alpha^2 \rangle - \langle v_\alpha \rangle^2 \right), \tag{19}$$

where k is the Boltzmann constant and m_{H} the mass of hydrogen atom; it can be easily shown that for the sight lines laying in the reference plane

$$\begin{aligned} T_\alpha \; &= \; T_r \cos^2\alpha + T_{\rho,1} \sin^2\alpha + \\ &+ \; \frac{m_{\mathrm{H}}}{k} \left(\langle v_r v_{\rho,1} \rangle - \langle v_r \rangle \langle v_{\rho,1} \rangle \right) \sin 2\alpha. \end{aligned} \tag{20}$$

T_r and $T_{\rho,1}$ are local radial and perpendicular temperatures, defined by the formulae:

$$T_r = \frac{m_{\mathrm{H}}}{k} \left(\langle v_r^2 \rangle - \langle v_r \rangle^2 \right), \tag{21}$$

$$T_{\rho,1} = \frac{m_{\mathrm{H}}}{k} \left(\langle v_{\rho,1}^2 \rangle - \langle v_{\rho,1} \rangle^2 \right). \tag{22}$$

In this notation the classical definition of temperature is the following:

$$T = \frac{m_{\mathrm{H}}}{3k\, n_{\mathrm{H}}} \iiint\limits_{v} (\boldsymbol{v} - \boldsymbol{v}_{\mathrm{B}})^2 \, \tilde{f}_{\mathrm{H}} \, \mathrm{d}^3 v, \tag{23}$$

although because of the strongly anisotropic character of the distribution function (which will be discussed later) this parameter is of limited practical value.

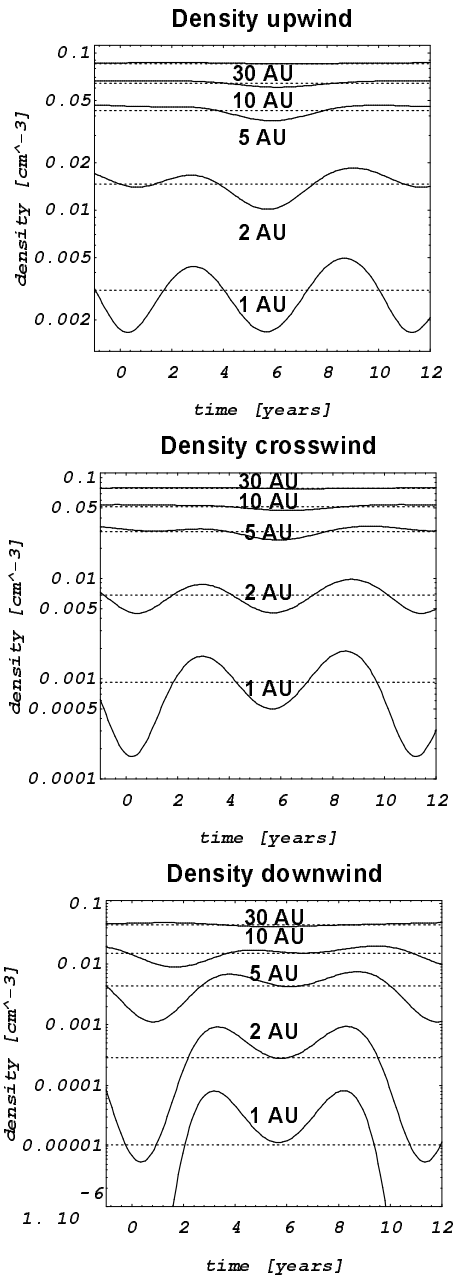

Fig. 2. Variation of hydrogen density presented at selected heliocentrtic distances for the upwind (upper panel), crosswind (middle panel) and downwind (lower panel) directions during the solar cycle. Time 0 corresponds to the maximum solar activity epoch. The dotted horizontal lines represent the density levels given by the MSM model, the vertical axis is in the log scale.

4. Solar cycle variation of local density, bulk velocity and temperature of interplanetary hydrogen

4.1. Density

The variation of neutral hydrogen density during the solar cycle has already been extensively discussed by Ruciński & Bzowski (1995) and Bzowski & Ruciński (1995a,b), so here we present only a brief review.

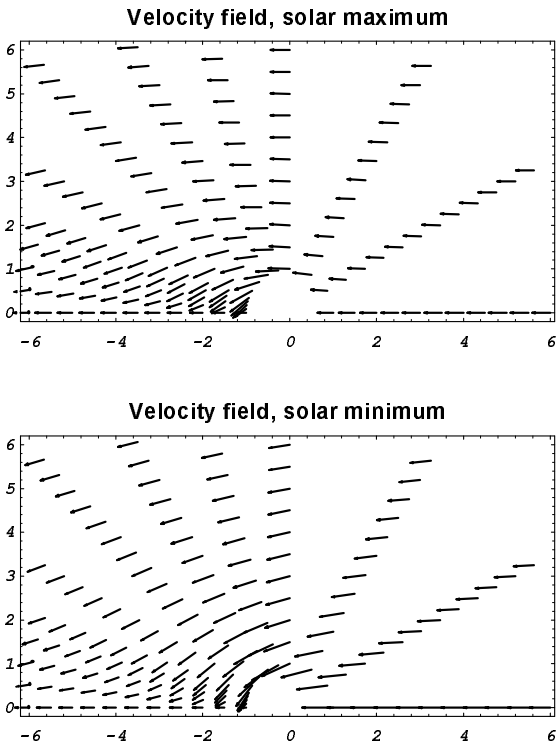

Fig. 3. Local bulk velocity field for solar maximum (upper panel) and solar minimum (lower panel). The upwind direction is to the right, the axes are scaled in astronomical units with the Sun at the point (0,0). Note that despite during the solar maximum epoch the net force acting on individual atoms is repulsive, the flow of the gas in the downwind region generally converges to the symmetry axis.

The variability of density is quite strong near the Sun, but it fades off rapidly with the increasing heliocentric distance in the upwind hemisphere, smearing out between 5 and 10 AU (see Fig. 2). In the downwind direction it is very pronounced near the Earth's orbit, its amplitude being several orders of magnitude. Significant variations continue in that region out to about 20 AU. It is worth to note that the density variations are quite strong within the so-called Maximum Emissivity Region (MER), i.e. at the location where the Lyman-α resonance emissivity (source function of the gas), proportional to the term $n(r)/r^2$, attains its maximum value.

4.2. Bulk velocity

In this section the local bulk velocity of neutral hydrogen within the inner heliosphere will be discussed. The full bulk velocity is indicative of the local dynamic time scale in the travelling gas but usually it is not directly observable. The observable quantity may be the projection of bulk velocity on the line of sight of a spectrally sensitive Lyman-α detector. The bulk velocity of the gas in the static case was discussed by Lallement et al. (1984) and the qualitative conclusions drawn by these authors agree with the conclusions reached here.

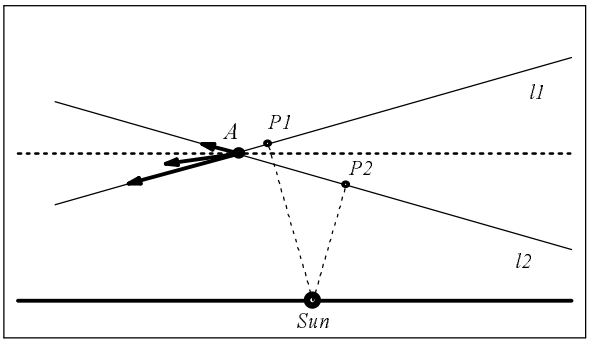

Fig. 4. Schematic illustration of the effect of deflection of the bulk flow towards the symmetry axis in the region behind the Sun.

The velocity field of the gas at the epochs of maximum and minimum of the solar cycle is presented in Fig. 3. The bulk velocity of the gas is a statistical quantity and must not be mistaken with the velocities of individual atoms. The actual atomic trajectories are hyperbolae attracted or repelled by the joint action of solar radiation pressure and gravity while the local bulk velocity vector of the gas is a composition of many different atoms coming from different directions at different speeds with different probabilities. Therefore the local bulk velocity vector field appears quite different than one might intuitively expect. During solar maximum, when the net force acting on the atoms is repulsive, one does not find a collective outward deflection of the gas, even for the positions around 90° off the inflow axis, apart from the regions very close to the Sun; instead the bulk of the gas seems to flow consistently towards the symmetry axis. Among the atomic trajectories the vector field of bulk velocity is composed of, one can distinguish the 'direct' and 'indirect' ones (for definition see e.g. Lallement et al., 1985). They form two more or less independent streams which do not interact because the gas is collisionless; the intensities of the streams are comparable in the downwind region and their direction depends strongly on the position in space. They are not depicted in the figure because in the analysis performed in this paper there was no differentiation between direct and indirect atoms.

The explanation of the flow depicted in Fig. 3 is quite simple. Let us assume for the moment that the solar radiation pressure exactly compensates the solar gravity and let us consider a point A, as indicated in Fig. 4. In the absence of the effective force any atom would follow a straight line trajectory. Let us select a pair of atoms following trajectories l_1 and l_2, as indicated in the figure. From the dynamical point of view the two trajectories have equal probabilistic weights. However, when the atoms reach the point A, the atom from l_2 has a lower weight than the atom from l_1 because it has already passed its perihelion point P_2, which is closer to the Sun than that of the atom from l_1. Since the ionisation rate depends on the heliocentric distance r as $1/r^2$, from the couple of atoms travelling from "infinity" at the same speed the lower probability weight has the one that has approached closer the Sun. In this particular case this is the atom from l_2. To compute the contribution of the couple of atoms to the bulk

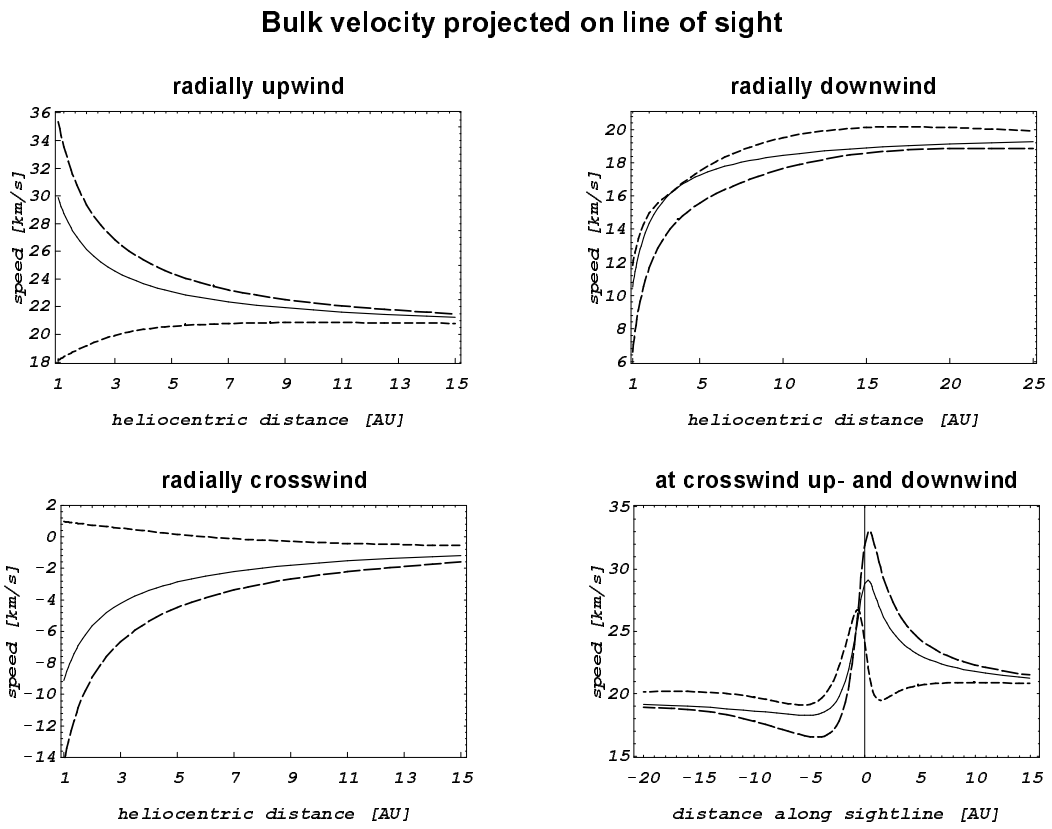

Fig. 5. Projection of hydrogen bulk velocity on different lines of sight. The lines of sight from the panels in the left-hand column and the upper right position are directed radially away from the Sun and start at 1 AU in the positions indicated in the panel headers. In the lower right panel velocity projections on two sightlines are shown. Both originate at 1 AU in the crosswind position and are parallel to the inflow axis; one of them is directed upwind (positive distances from the observer), and the other one downwind (negative distances). The solid lines in all panels correspond to the MSM case, the short-dash line to the solar cycle maximum, and the remaining one to the solar cycle minimum.

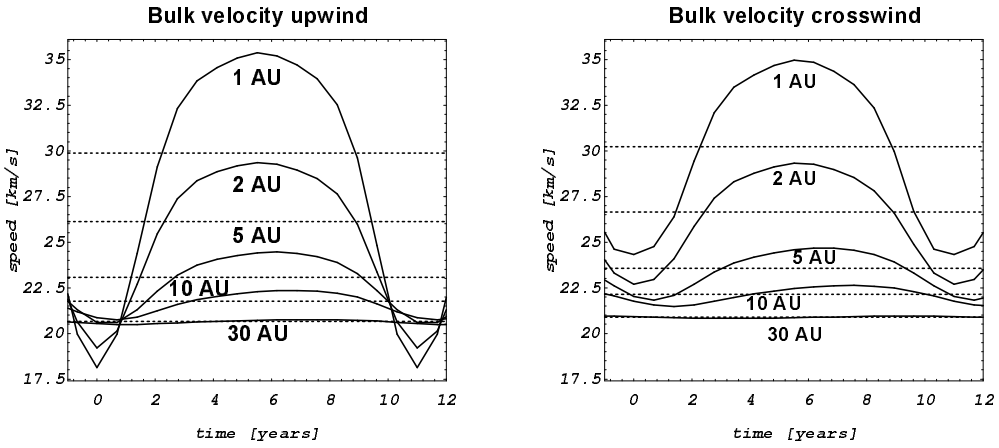

Fig. 6. Variations of bulk velocity at selected heliocentric distances upwind and crosswind during solar cycle. The dotted horizontal lines represent appropriate MSM velocities. Time equal 0 corresponds to the maximum solar activity epoch. Total bulk velocity in the upwind direction is equal to the radial velocity along this axis.

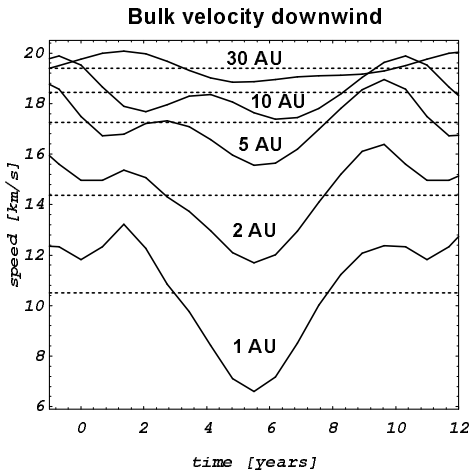

Fig. 7. Variations of bulk velocity downwind at selected heliocentric distances during solar cycle. The dotted horizontal lines represent appropriate MSM velocities.

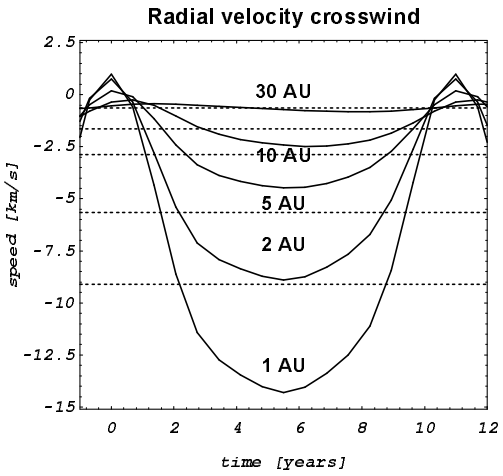

Fig. 8. Variations of radial component of bulk velocity crosswind at selected heliocentroc distances during solar cycle. The dotted horizontal lines represent appropriate MSM values.

velocity of the gas at A we take their velocities with appropriate probability weights, and because the probability weight of the atom from l_1 is larger, the resulting vector for net bulk velocity is tilted towards the symmetry axis even though there is no actual force acting on individual atoms.

A similar reasoning permits to understand why there is a general increase in bulk speed of the gas near the Sun even though the net force acting on the atoms may be zero: the ionisation eliminates by higher rates those ones that traverse the inner Solar System with slower velocities and thus remain in this region for a longer time. The faster atoms have a better chance to survive the approach to the Sun, so after passing by the Sun the proportion of the faster atoms to the slower ones in the statistical ensemble is higher than before.

In fact, the hydrogen bulk velocity is driven by two phenomena: (i) the joint action of solar gravity and radiation pressure, and (ii) the ionisation. In the upwind hemisphere, stronger radiation pressure and weaker ionisation tend to reduce the bulk velocity and weaker radiation pressure and stronger ionisation to increase it. In the downwind hemisphere the situation is different, the bulk speed is increased by an increase of both ionisation rate and radiation pressure.

The bulk velocity is only slightly affected beyond ~ 10 AU. In the MSM model at 30 AU its deviations from the initial inflow velocity do not exceed 5%, and 10% at 10 AU. Closer to the Sun, however, the departures of bulk velocity from the initial value become quite pronounced; for example, in the MSM model at 1 AU they attain +20 km/s upwind and -8 km/s downwind.

Similar behaviour is demonstrated by radial velocity, which in the crosswind direction (i.e. 90° off the inflow axis) at 30 AU is equal to only -0.5 km/s, but at 1 AU it attains in MSM -9 km/s. The profiles of bulk velocity upwind, downwind and crosswind for the MSM model are presented in Fig. 5. They are in quantitative agreement with the results of Wu & Judge (1979) who adopted different values of radiation pressure and ionisation rate.

From the observational point of view it could be of interest to see the velocity of the gas along some selected lines of sight, coinciding with typical measurement geometries. It is, of course, impossible to present here all possible geometries, but we believe it would be illustrative to consider the geometry used for demonstrative purposes by Scherer & Fahr (1996) and Wu & Judge (1980). Let us consider vantage points at 1 AU from the Sun located upwind, crosswind, and downwind, i.e. at the angles 0°, 90° and 180° off the inflow direction, respectively. The lines of sight from these locations would be directed radially away from the Sun; additionally, at the crosswind vantage point let us take the sightlines directed parallel to the inflow axis and going upwind and downwind.

The projections of bulk velocity on these lines of sight are presented in Fig. 5. One can hardly treat the gas observed in this geometry as constant in speed. The difference between maximum and minimum values of velocity projections on the selected sightlines in the MSM case is at least 15 km/s, that is more than the thermal spread of the gas "at infinity", equal to about 11.5 km/s. What is more important, the velocity profiles are the steepest in the regions close to the positions of maximum of optical source function along the relevant lines of sight.

The introduction of variability of radiation pressure and ionisation rate considerably modifies the picture. While in general the region where the bulk velocity is altered by solar radiation pressure, gravity, and ionisation does not change, there appear significant variations of the magnitude of velocity and of its direction. In several cases the variability introduces differences where they did not exist in the static case, and in some cases the differences are reduced. A good example can be seen in Fig. 6, where the variations of total bulk speed at various heliocentric distances upwind and crosswind are presented. The velocity in the time-dependent case is highly variable up to heliocentric

distances of $\sim$ 5 AU, there exist noticeable differences in the variability patterns, particularly within 2 AU from the Sun just after and before the solar maximum epoch. The variations at 1 AU may reach +5 and -10 km/s upwind and ± 5 km/s crosswind relative to the MSM level; at 5 AU they are reduced to just ± 3 km/s both upwind and crosswind.

The bulk velocity is variable up to much larger distances in the downwind region, as it is evident in Fig. 7. The variability at 1 AU is equal to about $\pm 40\%$ of the MSM value, though one should keep in mind that the gas density in this region is extremely small. At 10 AU the deviations from the MSM velocity are still about 15% and continue down to 30 AU at about 10%. The course of variations is rather complicated and reflects the complex dynamic and ionisation history of the contributing atoms.

For spectral observations the relevant quantity is the projection of the bulk velocity of the gas on the selected line of sight. For an observer located at the inflow axis in the upwind and downwind positions and looking away from the Sun the bulk velocity has only the radial component, defined in Eq. (7). For an observer at the crosswind position the profiles of radial velocity over the solar cycle at various heliocentric distances are presented in Fig. 8. Also this quantity is strongly variable and the strongest variations occur in the region giving considerable contribution to the results performed from 1 AU from the Sun.

Another observing geometry might be the one already presented during the discussion of the MSM model: observations performed from the crosswind position at 1 AU. The projection of bulk velocity on the line parallel to the inflow axis and separated by 1 AU are presented in Fig. 5. The presented profiles of velocity projection demonstrate that also in this geometry the variability of bulk velocity is quite strong, especially in the upwind region, where the majority of the Lyman-α backscattered glow comes from. At 1 AU from the detector they are about $+20/-50\%$ and they more or less converge to the MSM profile at about 10 AU.

A factor affecting the shape of backscattered radiation spectral lines is the change of radial velocity along the sightline. This quantity is strongly seasonal and throughout the heliosphere it is the weakest around solar maximum and the strongest around solar maximum. In the upwind hemisphere the change of radial velocity along radial sightlines during solar maximum is just 1 to 2 km/s and at the downwind axis it increases to about 8 km/s; because of the particular courses of variability of radiation pressure and ionisation rate adopted in this modelling one can even find solar cycle phases when there is practically no change in radial velocity along radial sightline at all: this situation occurs about 1 year before and after the maximum. In the "offset geometry" discussed earlier the changes of radial velocity are a little higher and reach about 6 km/s. Thus one can infer that around solar maximum the width of the spectral line of backscattered radiation observed along lines of sight directed radially away from the Sun is essentially determined by the thermal spread of the gas.

During solar minimum the differences are quite big and in the upwind and downwind directions they may exceed 15 km/s; in the "offset geometry" they are slightly smaller but still comparable to or greater than the thermal spread of the gas. It is interesting to note that even in the crosswind direction the differences in radial velocity during solar minimum are not small and attain about 12 km/s. These inhomogeneities in velocity along lines of sight tend to broaden the spectral lines of Lyman-α backscatered radiation.

4.3. Temperature

The temperature of interstellar hydrogen within the inner heliosphere has up to now been studied only in the static case (Wu & Judge 1979, 1980; Lallement et al., 1984). To interpret optical observations one needs to know the thermal spread of the gas along the sightline of the detector. In observations along heliocentric lines of sight the spread measure is the radial temperature defined in Eq. (21), as considered by Wu & Judge (1979, 1980); for other sightlines one has to compute the projection of temperature tensor onto appropriate lines of sight according to Eq. (18). The radial temperature along selected sightlines is presented in Fig. 9. The gas is by no means isothermal. In the MSM case in the upwind direction the change of temeprature along radial lines of sight within 15 AU from the Sun is about 2000 K (from about 5 000 K at 1 AU to about 7 000 K at 15 AU), in the crosswind direction only about 300 K and in the downwind direction about 4000 K within 25 AU. The temperatures in the downwind direction are consistently higher by about 4000 K than in the upwind direction. The results obtained in this study for the radial temperature in the static case are in very good agreement with the results obtained by Wu & Judge (1980); one should remember, however, that the parameters of the model used in their paper were slightly different, preventing direct comparison.

In the variable case the change of temperature along radial sightlines is strongest around solar minimum epoch and equal to about 3000 K in the upwind and crosswind directions and to about 5000 K in the downwind direction. In the "shifted geometry" (lines of sight directed upwind and downwind from the position at 90° off the inflow axis and at 1 AU from the Sun) the change of radial temperature upwind and downwind is equal, respectively, 1200 and 2000 K in the MSM case, 1000 and 1000 K around solar maximum, and 2000 and 3500 K around solar minimum. Similarly as in the case of radial velocity, the smallest change of temperature along radial sightlines occurs around solar maximum and, as before, due to particular courses of radiation pressure and ionisation rate adopted in this modelling, at about 1 year before and after the solar maximum the gas along the radial sightlines in the upwind hemisphere is almost isothermal, in contrast to the solar minimum epoch, when the change is the most pronounced.

The variation of radial temperature during solar cycle at selected heliocentric distances is presented in Fig. 10. In general, the course of temperature in time is a mirror reflection of the course of bulk velocity (cf. Figs. 6, 7, and 8). Where one could observe the velocity maximum, one observes the temperature minimum and vice versa.

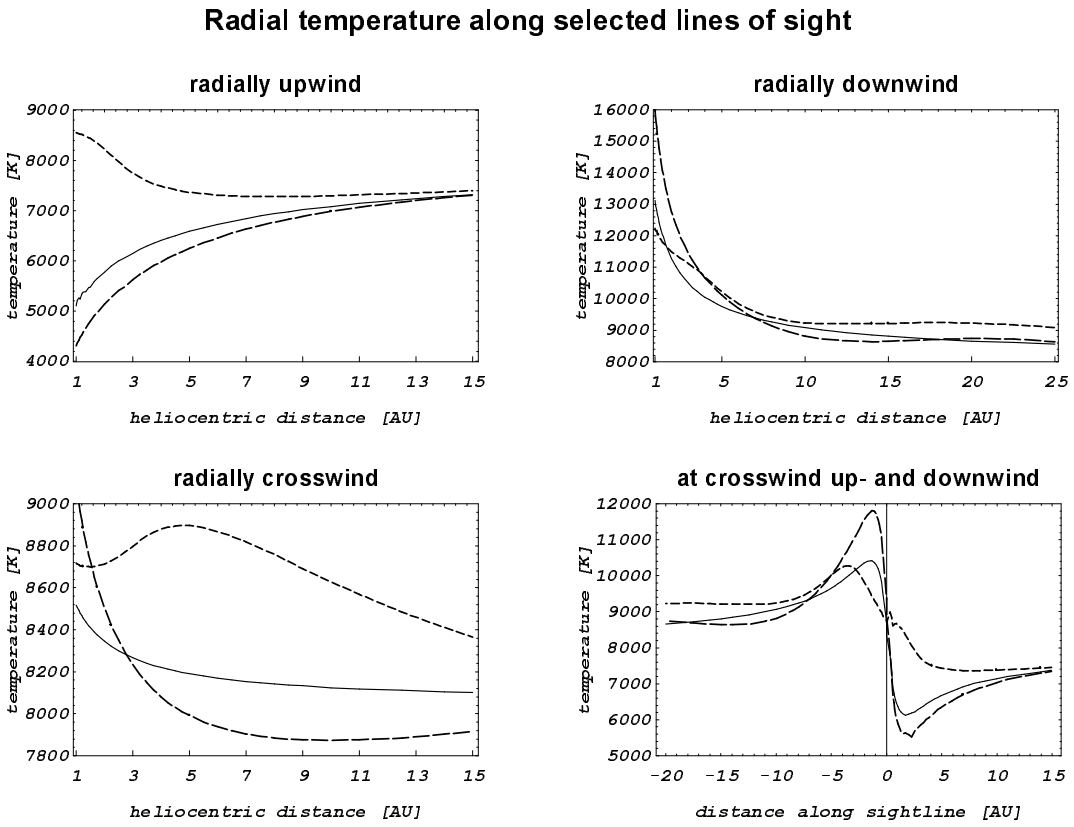

Fig. 9. Radial temperature of interplanetary hydrogen for selected lines of sight. The lines of sight from the panels in the left-hand column and in the upper right position are directed radially away from the Sun and start at 1 AU in the locations indicated in the panel headers. In the lower right panel velocity projections on two sightlines are shown. Both originate at 1 AU in the crosswind position and are directed parallel to the inflow axis: one of them upwind (positive distances from the observer), and the other one downwind (negative distances). The solid lines in all panels correspond to the MSM case, the short-dash line to the solar cycle maximum, and the remaining one to the solar cycle minimum.

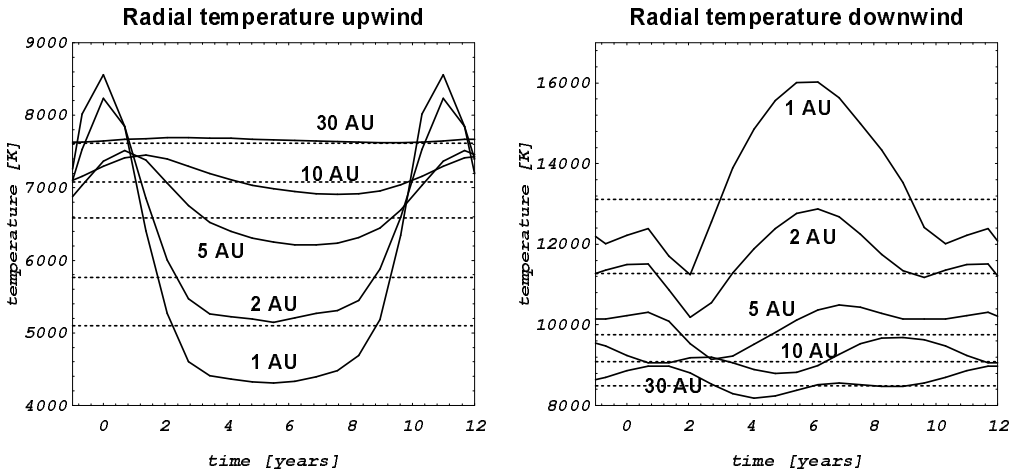

Fig. 10. Radial temperature upwind and downwind during solar cycle at selected heliocentric distances. The variable case is drawn with solid lines, MSM case with broken lines.

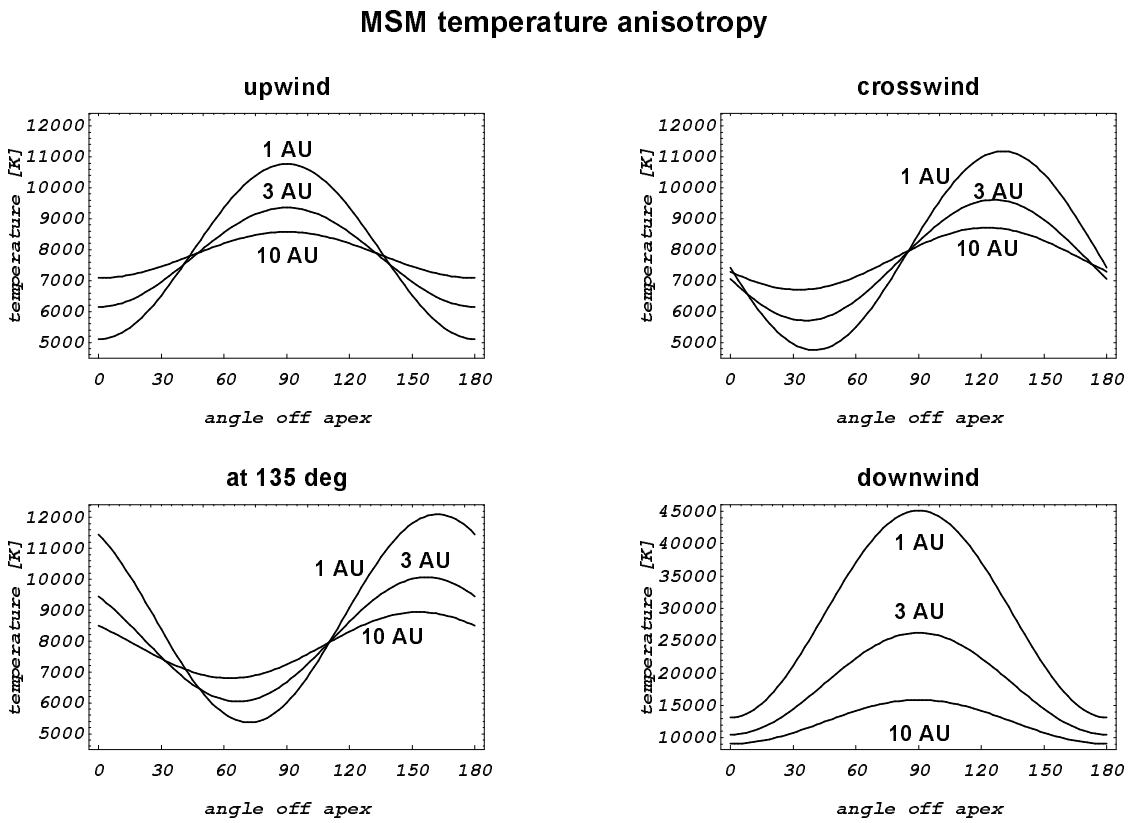

Fig. 11. Illustration of the anisotropy of temperature in the MSM case at various locations in space. The projections of temperature tensor on various axes inclined to the apex direction at the angle α indicated in the horizontal axes. The heliocentric distances of the vantage points are indicated at the appropriate curves and their position angles off the apex direction in the panel headers. The projections were computed from Eq. (20).

The picture of radial temperatures presented in Fig. 9, i.e. along the lines of sight partly investigated in the earlier studies (see e.g. Wu & Judge 1979), is deceptively simplistic. Even in the MSM case the thermal spread of the gas along various lines of sight is strongly anisotropic. Some of this anisotropy is presented in Fig. 11. The temperature tensor is truly three-axial and the orientation of its longest axis depends on the position within the heliosphere and on the phase of the solar cycle. For a given heliocentric distance in the stationary case the anisotropy is weakest at the upwind axis and it increases with the offset angle, reaching maximum at the downwind axis. The sharp increase of temperature and anisotropy in the tail region is caused by the fact that in this region the counterflowing streams of atoms from the flanks are meeting. The anisotropy ratio in the MSM case, computed as the ratio of axes of temperature tensor in the reference plane in a given location in space, drops down from about 2.0 and 3.5 at 1 AU to about 1.1 and 1.6 at 20 AU upwind and downwind, correspondingly.

The anisotropy of the temperature tensor is caused by the anisotropy of the distribution function. The thermal character of the gas makes the distribution function similar to a three-axial Maxwellian. It does not resemble the ring-like structure presented by Kyrölä et al. (1994) for the case of cool ($\sim$ 80 K) gas; for the temperature "at infinity" equal to 8000 K the projection of the distribution function on the reference plane (i.e. the distribution function integrated over κ) is an arc-like hill with moderate slopes. A section of this hill along a straight line may in some cases produce a two-peak structure.

The increase of temperature computed from Eq. (19) along some lines of sight in the downwind region is not fully caused by heating by solar factors. Some of the "apparent thermal spread" is caused by the presence of the 'direct' and 'indirect' populations discussed in the velocity section which are responsible for a two peak structure of the distribution function along some section lines. Therefore the projection of the temperature tensor defined in Eq. (19) on an arbitrarily selected line is not an adequate measure of the thermal spread of the whole population. The exception is the radial temperature as defined in Eq. (21) for a line of sight directed along the downwind axis. Because of the axial symmetry, the radial components of the streams of atoms intersecting the downwind axis are identical and the section of the distribution function along the downwind axis is single-peak, thus enabling treatment of the spread defined in Eq. (21) as thermal. Since no differentiation of atoms between the 'direct' and 'indirect' channels was made in this paper, we leave a more thorough discussion of this question to a future work.

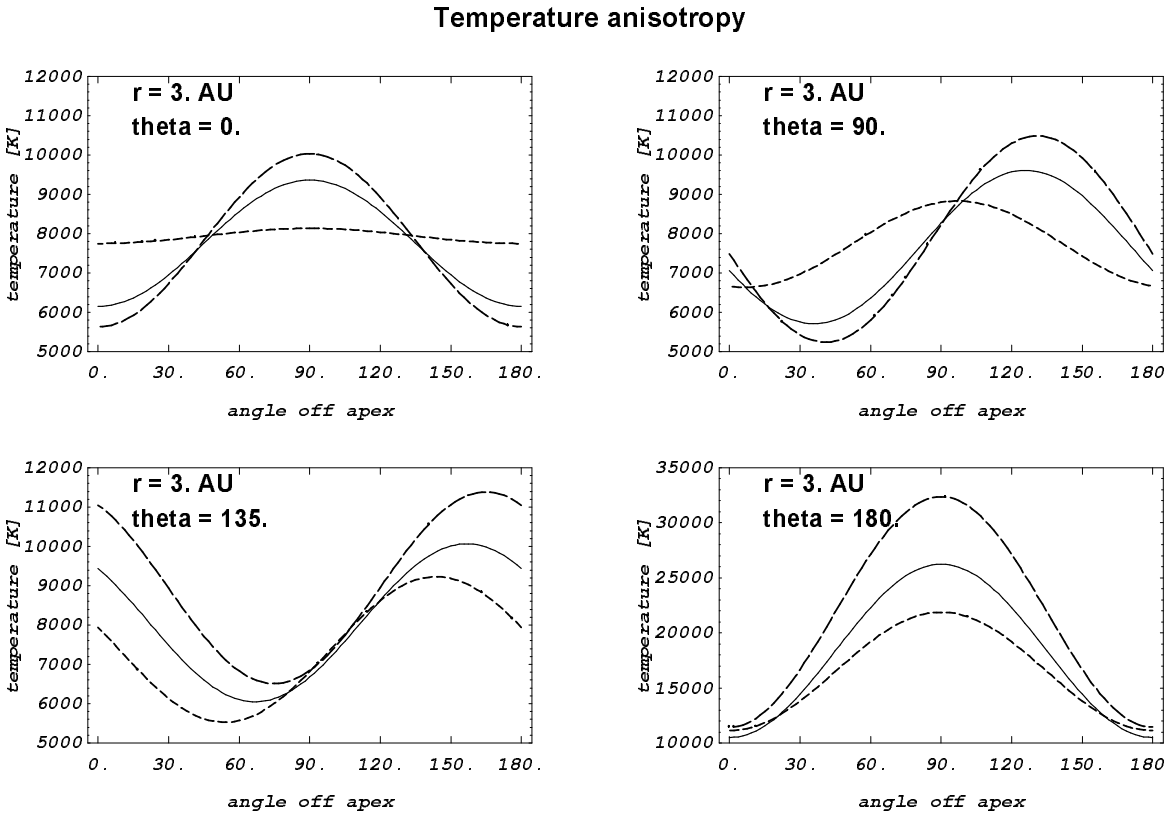

Fig. 12. Illustration of temperature anisotropy and its variations during solar cycle. Presented are projections T_α of temperature tensor on lines of sight inclined to the inflow direction at the angles α indicated in the horizontal axes, computed from Eq. (20). The locations of vantage points in space are indicated in the panels. Their heliocentric distance was chosen at 3 AU so that they remain close to the Maximum Emissivity Region in the upwind hemisphere. Note that the vertical scale in the lower right (downwind) panel is different from the scale in the other panels. The solid lines correspond to the MSM case and are identical as the 3 AU lines in Fig. 11; the short-dash lines correspond to the variable model, solar maximum conditions, and the long-dash lines to the variable model, solar minimum conditions.

Both the anisotropy ratio and the direction of the longest axis of temperature tensor vary during the solar cycle. This effect is illustrated by some examples in Fig. 12. The direction in space of the longest axis of temperature tensor shows some correlation with the local direction of the gas flow but not a hundred percent one. For a given heliocentric distance the anisotropy ratio increases with the angle off the upwind direction and it is in general larger during solar maximum.

The fact of that sort of variability of temperature tensor may prove important during interpretation of observations of interplanetary backscattered Lyman-α radiation, particularly for the lines of sight which are not directed radially away from the Sun, and it certainly deserves examination. Special care is needed particularly in the downwind hemisphere, where the projections of the temperature tensor to different lines of sight may vary from about 10 000 K to more than 35 000 K, what translates into variation in thermal speed from about 12.8 to 24 km/s. The significance of the temperature anisotropy for interpretation of observations made from about 1 AU and from the regions beyond about 15 AU in the upwind region and about 25 AU in the downwind region seems to be small because in the first case the projection of temperature tensor on the line of sight due to geometric conditions is for the most part of the sightline not very much different from the radial temperature computed from Eq. (21), and in the second case the anisotropy itself is not very strong.

The velocity and temperature fields computed using the presented model do not depend at all on density "at infinity" and the response of the density field to the change of assumed density "at infinity" n_0 is linear. This would not have been the case had filtration effects at the heliospheric interface been taken into account.

5. Practical application: consequences on observations of backscattered Lyman-α radiation

The discussion up to now has had a strictly theoretical character. An important question is whether the presented phenomena can somehow be detected by observations. To start with let us consider the source function of the interplanetary hydrogen gas at a selected phase of the solar cycle under the assumption that the solar Lyman-α line profile is flat and that complete redistribution of the Lyman-α photons takes place.

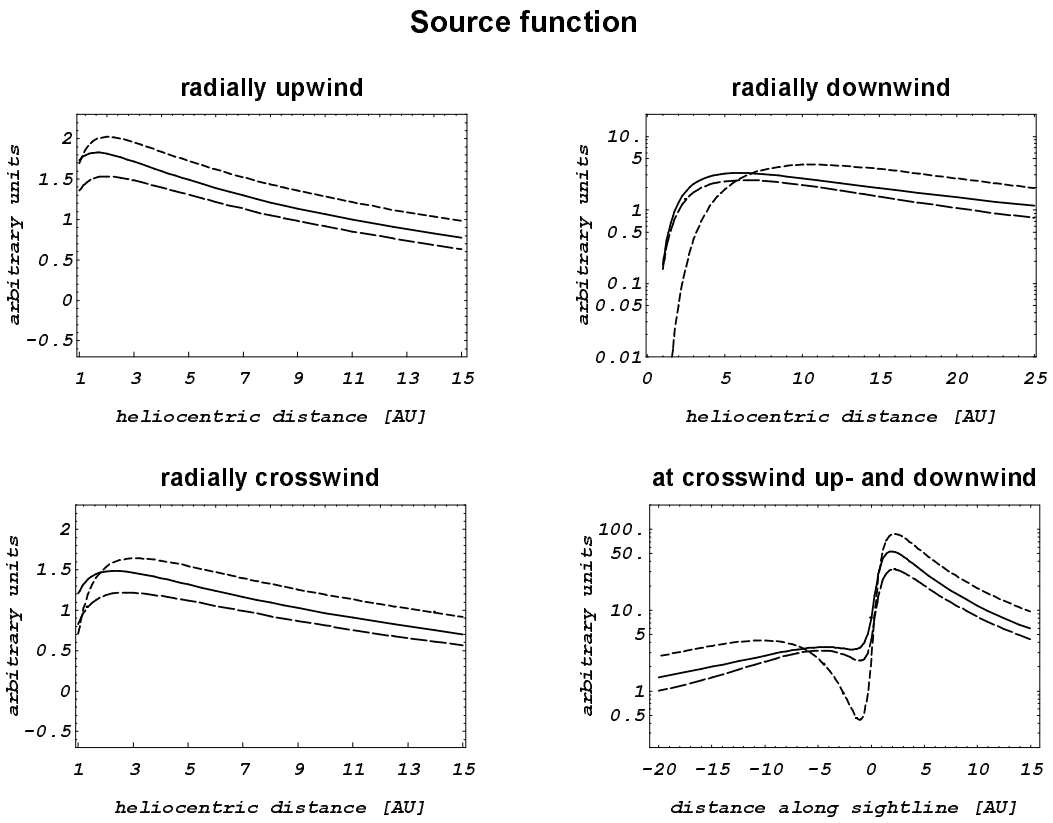

Fig. 13. Source function of interplanetary hydrogen for upwind, crosswind and downwind positions at 1 AU. In the upper row the function is presented for the lines of sight directed radially away from the Sun from the positions upwind and downwind and in the lower row it is presented for the crosswind position; in the left-hand panel for the line of sight directed radially away from the Sun and in the right-hand panel for the lines of sight directed parallel to the upwind and downwind directions. The solid curves correspond to the MSM model, the short-dash curves to the variable model during the solar maximum epoch and the long-dash curves to the solar minimum epoch. The units are arbitrary but they make possible a cross-comparison of the function values between panels. The maxima of the function determine the position of Maximum Emissivity Region for a given line of sight.

For an observer at a point (r_0, θ_0) the source function at a point (r_i, θ_i) is defined as follows:

$$S_i = I_0\, n_{\rm H}\,(r_i, \theta_i) \left(\frac{r_0}{r_i}\right)^2 \sigma_{\rm tot}\, V\left(T_{r,i}\,(r, \theta)\right)\ \Phi\,(\theta_i)\,, \tag{24}$$

where I_0 is the spectral solar Lyman-α intensity at r_0 during observation, $\sigma_{\rm tot}$ is the integrated atomic cross section for resonance scattering of Lyman-α photons, given by the formula:

$$\sigma_{\rm tot} = \frac{\pi e^2 f}{m_{\rm e} c^2}, \tag{25}$$

Φ is the dipole phase function for resonance scattering, and defined by the formula

$$\Phi(\theta) = \frac{3}{4}\left(1 + \cos^2\,\theta\right), \tag{26}$$

and $V(T_r)$ is the Voigt function, computed from the formula:

$$V(T_r) = \frac{a}{\pi} \int\limits_{-\infty}^{\infty} \frac{\exp\left(-x^2\right)}{a^2 + (1 - x)^2}\,{\rm d}x, \text{ and } a = \frac{\Delta\lambda_0}{\lambda_0 \sqrt{\frac{2k\,T_r}{m_{\rm H} c^2}}}. \tag{27}$$

The source function integrated along selected sightlines brings the intensity that would be observed by a spaceborne detector.

Our computations reveal that the dependence on temperature of the source function in the form defined by Eqs. 24 to 27 is very weak. The only term directly dependent on temperature is the Voigt function which in the temperature range from 8 000 to 50 000 K changes by less than 0.1%. Therefore, since the assumption of the flat solar line profile introduces no dependence of the source function on bulk velocity, the only source of its variability is the variability of density, and hence the results of the discussion of the emissivity function already presented by Ruciński & Bzowski (1995) apply to the source function case. Qualitatively, they are not changed in the case of lines of sight at the crosswind position directed parallel to the inflow axis.

The source function of interplanetary hydrogen along the sightlines originating at 1 AU in the upwind, crosswind, and downwind positions is presented in Fig. 13 for the solar cycle maximum and minimum epochs and, for comparison, for the MSM case.

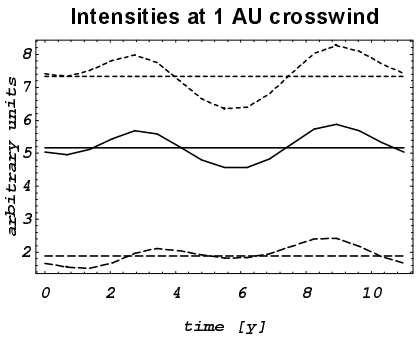

Fig. 14. Course of intensity of the Lyman-α backscattered radiation observed from 1 AU in the crosswind position during solar cycle. The solid curve corresponds to the line of sight directed radially away from the Sun, the short-dashed curve to the line of sight directed upwind parallel to the inflow direction and the long-dashed curve to the line of sight directed downwind parallel to the inflow axis. The horizontal lines reflect the MSM values.

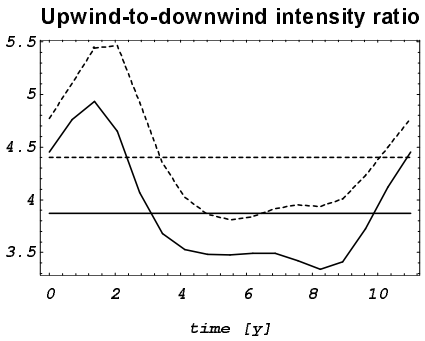

Fig. 15. Upwind-to-downwind intensity ratio during the solar cycle. The solid curve corresponds to the ratio of intensities observed at 1 AU from the upwind and downwind positions along the lines of sight directed radially away from the Sun, and the broken line to the ratio of intensities observed from the crosswind position along the lines of sight parallel to the inflow axis and directed upwind and downwind. The horizontal lines correspond to the appropriate intensity ratios derived from the MSM model.

The optical quantity most often observed during the past studies of Lyman-α backscattered radiation is the total intensity. As it has already been stressed by Bzowski & Ruciński (1995b) and Ruciński & Bzowski (1995), even in this simple optical model the variation of backscattered intensity arises not only because of the variation in the Lyman-α ilumination, but also because of the variability of hydrogen density distribution. This effect is illustrated in Fig. 14, where the course of backscattered intensity, normalised by the illumination factor $\mu(t)$ from Fig. 1, is presented for the vantage point at 1 AU in the crosswind position. Intensities collected along the upwind, crosswind and downwind lines of sight are shown. One can assess from the figure their relative strength and observe that (i) the variability of density distribution is responsible for variability in intensity of about 15 to 30% around the MSM level (in this particular case), and (ii) the maximum departures from the stationary case do not occur during the solar maximum or minimum epoch (particularly for lines of sight in the downwind direction).

The interpretation of actual observations provided in the literature revealed the problem of discrepancies in the upwind-to-downwind intensity ratio between the values expected from the static "hot" model and the values observed. Our analysis proves that this quantity is also highly variable during the solar cycle. Its course is independent of the actual solar illumination and therefore is the direct tracer of non-stationary effects caused in the interplanetary hydrogen by the solar variabilities. It seems that the best vantage point to observe this quantity is at crosswind because from there one can register the downwind and upwind intensities at the same time.

The course of the upwind-to-downwind intensity ratio for these positions is presented in Fig. 15. The two courses are similar in appearance. The departures from the MSM level in both cases are about 25% and the maximum amplitude occurs during the intermediate solar cycle phases. This effect can be attributed to the anticorrelation of the radiation pressure and ionisation rate functions adopted in our model. However, removal of the anticorrelation would not remove the variability of the upwind to downwind intensity ratio itself.

A more sophisticated analysis, based on the radiation transfer model by Scherer & Fahr (1996), reveals further interesting effects. The variability of local bulk speed and temperature is reflected by both the spectral profile and the Doppler shift of the backscattered radiation. Some examples for that can be seen in Fig. 16. The profiles were computed taking into account the radial temperature, bulk velocity, and density of interplanetary gas and their variations and assuming that the illuminating beam is constant in time. This permits to judge the variability introduced to the shapes of the profiles by the time-dependent effects present in the gas itself and not caused by momentary variations in the solar Lyman-α output. One should keep in mind, however, that the line shapes could be different had one taken into account the fact that the shape of the solar Lyman-α line may vary during the solar cycle. This phenomenon is, however, poorly investigated and therefore has been excluded from this study.

A procedure that is often used when interpreting observed interplanetary Lyman-α lines is to fit a Gaussian to the observed profiles. While in principle the profile should better be fitted to a Voigt function, due to low signal-to-background ratio, typical for interplanetary line observations (see e.g. Scherer & Fahr 1996), the Gaussian profile, given by Eq. (28), is sufficient.

$$I(\lambda)\mathrm{d}\lambda = I_0 \frac{1}{\sqrt{\pi}\Delta\lambda_\mathrm{D}} \exp\left[-\left(\frac{\Delta\lambda}{\Delta\lambda_\mathrm{D}}\right)^2\right] \mathrm{d}\lambda, \tag{28}$$

$\Delta\lambda_\mathrm{D}$ is the Doppler width of the profile and equal to:

$$\Delta\lambda_\mathrm{D} = \frac{\lambda_0}{c}\sqrt{\frac{2kT}{m_\mathrm{H}}}; \tag{29}$$

$\Delta\lambda = \lambda - \lambda_0$, where λ_0 is the wavelength of line centre which is usually Doppler-shifted. The profile has three free parametrs: I_0,

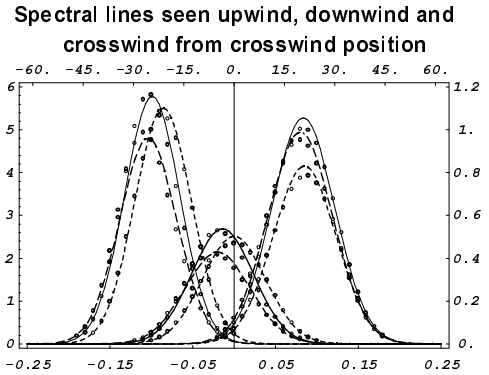

Fig. 16. Spectral lines of the backscattered radiation computed from the model data presented in this paper. Dots correspond to the profiles computed using the optical code by Scherer & Fahr (1996), curves to the Doppler profile functions specified in Eq. (28), fitted to the relevant profile data sets. The vantage point is at 1 AU in the crosswind position, the profiles at the left-hand side of the figure correspond to the line of sight directed upwind, the profiles in the middle to the line of sight directed radially away from the Sun, and the profiles at the right-hand side to the line of sight directed downwind. The vertical axes are scaled in arbitrary units and the left-hand scale corresponds to the upwind and crosswind profiles and the right-hand scale to the downwind profiles. The wavelength scaled in Å is presented at the lower horizontal axis; the upper horizontal axis is scaled in units of Doppler speed (km/s). Zero wavelength (zero Doppler speed) correspond to the laboratory wavelength of Lyman-α line, equal to 1215.66 Å. The profiles drawn with the solid line correspond to the MSM model and the ones drawn with broken lines to the time dependent model: the short-dashed one to the solar cycle maximum conditions and the long-dashed to the solar minimum conditions.

$\Delta\lambda_{\rm D}$, and λ_0. The Doppler shift of the line can be expressed by as $v_{\lambda_0} = c(\lambda_0 - \lambda_{1215.66})/\lambda_{1216.66}$, and from the Doppler width of the line $\Delta\lambda_{\rm D}$ and Eq. (28) one can derive the temperature of the gas. The observable parameter is the full width at half maximum of the line, denoted here by $2\Delta\lambda_{1/2}$ and connected to the Doppler width and to the gas temperature by the formula

$$2\Delta\lambda_{1/2} = 2\sqrt{\log 2}\,\Delta\lambda_{\rm D} = 1.665\,\frac{\lambda_0}{c}\sqrt{\frac{2kT}{m_{\rm H}}}. \qquad (30)$$

This procedure was applied to profiles computed for selected lines of sight in the MSM case, for a few solar cycle phases in the variable model, and in the isothermal MSM case with the radial temperature artificially set to 8 000 K throughout the data set. The results are presented in Table 1 and Fig. 16.

The conclusions drawn from the table and from inspection of Figs. 5 and 9 are the following. The computed spectra of interplanetary lines very closely resemble Gaussian profiles – the correlation coefficients of the fits in all investigated instances exceed 0.99. One can observe, however, some skewness in the profiles which causes differences between the Doppler shift of the true maximum of the profile and the maximum of the fitted Gaussian profile equal to a few – about 2 or 3 – km/s; the shift from the Gaussian profile is always smaller than the shift from the "true" profile maximum.

Table 1. Doppler velocity and temperature derived from computed line profiles for selected radial lines of sight from 1 AU.

	upwind		crosswind		downwind	
	v[a]	T[b]	v	T	v	T
MSM	−24.4	7 840	−3.5	10 420	19.4	10 440
MSM iso T[c]	−24.8	9 480	−3.5	10 240	19.4	9 590
solar max	−21.3	8 320	0.0	10 710	21.3	10 210
1/4[d]	−25.0	8 260	−4.5	10 860	19.0	10 690
solar min	−26.5	7 680	−4.9	11 480	18.9	10 700
3/4[e]	−25.6	7 830	−4.7	10 910	19.0	10 980
MSM[f]	−24.4	8 200			20.6	10 700
MSM iso T[f]	−24.6	9 430			20.5	9 540
solar max[f]	−21.2	8 700			21.0	10 750
1/4[f]	−25.0	8 530			20.9	11 140
solar min[f]	−25.6	8 810			19.8	11 120
3/4[f]	−25.7	8 250			21.1	11 560

[a] Expressed in km/s.
[b] Expressed in K.
[c] MSM case with radial temperature artificially set to 8 000 K throughout in the data.
[d] Phase 1/4 of the solar cycle (half way between maximum and minimum).
[e] Phase 3/4 of the solar cycle (half way between minimum and maximum).
[f] From the crosswind position at 1 AU.

The Doppler shift of interplanetary lines observed upwind does not reflect the bulk velocity of the gas at distant regions of the Solar System (at about 30 AU from the Sun) but it is correlated with the solar cycle phase. The highest shift occurs during solar minimum and for the adopted parameters of the model it corresponds to the bulk velocity of about 26 km/s; the smallest one occurs during solar maximum and amounts to about 21 km/s. The Doppler shift of interplanetary lines observed downwind is almost independent of the phase of solar cycle and the apparent bulk speed is slightly less than 20 km/s, i.e. the adopted bulk velocity "at infinity". The profiles from the sightlines directed crosswind from the crosswind position are also Doppler-shifted throughout solar cycle except during the maximum phase. From the fact that the shifts of interplanetary lines in the MSM case and the isothermal MSM case (the iso T entry in Table 1) are practically identical one can conclude that spatial variation of temperature does not influence the fitted Doppler shift of interplanetary lines.

Another important conclusion is that the temperature derived from the full width at half maximum of an interplanetary line reflects neither the true radial temperature of the gas along the relevant line of sight, nor the temperature "at infinity". The correlation of this quantity with the solar cycle phase is weakly pronounced for all directions.

The width of interplanetary lines deserves some comments. Broadening of the line in comparison with the temperature of the gas is demonstrated by the profiles computed for the isother-

mal MSM case (the 'MSM iso T' entries in Table 1). While the temperature of the gas was set to 8 000 K and all the other variabilities of the gas, i.e. the bulk velocity and density, were left unchanged, the temperature derived from all spectral line widths is considerably higher than 8 000 K.

A spectral line has a perfect Gaussian profile when the gas is homogeneous, i.e. it does not have gradients in bulk velocity and temperature, and when the solar line can be considered as flat. Neither of these conditions is fulfilled in the case of interplanetary hydrogen, and all the departures from these conditions tend to broaden the line. The differences of bulk speed along the relevant lines of sight usually exceed 10 km/s and thus are similar to or greater than the thermal speed of the gas "at infinity". The radial temperature itself changes along a line of sight; while in the upwind hemisphere it decreases near the Sun, in the downind region it considerably increases. Furthermore, the profile of the illuminating solar Lyman-α line is self-reversed (see the relevant figure in Scherer & Fahr, 1996) and this, due to the Doppler shift of the flowing gas, causes departures of the profiles of resonance emission lines from the Gaussian shape. When the Doppler shift is small, as it is the case for the lines of sight directed radially away from the Sun from the crosswind position (the "crosswind" column in Table 1), the wings of the lines are enhanced and the temperature derived from the line width is increased.

As it comes out from Figs. 5 and 9, inhomogeneities in bulk veloctity and radial temperature of interplanetary hydrogen are weakest during solar maximum, at least in the upwind region. During that epoch spectral measurements of interplanetary resonance lines lead to the bulk velocity of the gas "at infinity" to within $\sim$ 10% and in case of the lines observed upwind, the temperature within $\sim$ 500 K.

The conclusions drawn for the MSM case are again in qualitative agreement with the conclusions from Wu & Judge (1980) worked out from an optically thin radiation transfer model, however, as it has already been mentioned, a direct comparison is impossible because of differences in the adopted parameter sets.

6. Conclusions

The main conclusions of this paper are the following. Interstellar hydrogen within the Solar System is not isothermal and has a strongly variable bulk velocity. The bulk velocity is increased not only by the joint action of solar gravity and radiation pressure but also by ionisation processes that eliminate more effectively slower atoms than faster ones. The changes in bulk velocity from "infinity" to about 1 AU from the Sun usually are of the order of 15 km/s or more and exceed the thermal speed of the gas.

The temperature of the gas is a tensor quantity and its degree of anisotropy and the magnitude and direction of the main thermal spread vary both in time and space throughout the heliosphere. The change of radial temperature along sightlines directed radially away from the Sun is about 3 000 K upwind and about 5 000 K downwind and is the strongest during solar minimum epoch; the weakest change occur during solar minimum.

The upwind-to-downwind ratio of intensity of the interplanetary Lyman-α resonance radiation varies during the solar cycle by about 20% around the mean value and it reaches the maximum value about 2 years after solar maximum epoch; the minimum value is reached in the second half of solar cycle but the exact timing depends on the position of the observer.

The bulk velocity and temperature derived from interplanetary backscattered radiation lines usually do not reflect the relevant parameters "at infinity". The inhomogeneities in the interplanetary gas are weakest within about 1 year around the solar maximum epoch and in case of observations made at this time one can expect an agreement of the bulk velocity derived from the Doppler shift of the line with the true velocity "at infinity" within $\sim 10\%$, during remaining phases of the solar system the Doppler shift of the lines observed in the upper hemisphere is larger; for the bulk speed "at infinity" equal to 20 km/s the speed derived from the Doppler shift is about 25–26 km/s.

The temperature derived from the width of interplanetary lines is closest to the true temperature of the gas "at infinity" in the case of observations carried out in the upwind direction. The differences do not exceed 500 K and are poorly correlated with the phase of the solar cycle. The temperatures derived from lines observed crosswind and downwind are overestimated by about 2 500–3 500 K; also in this case the correlation with the solar cycle phase is weak.

One should keep in mind that these conclusions are drawn based on model descriptions neglecting possible latitudinal dependence of charge exchange rate, photoionisation, and radiation pressure, as well as the filtration effects imprinted to the interstellar gas on its passage through the heliospheric interface, and furthermore, that the courses of radiation pressure that the model courses of radiation pressure and ionisation rate and their anticorrelation is only a rough approximation of reality. The conclusions concerning the width, Doppler shifts, and intensities of interplanetary lines are valid for the assumed value of neutral hydrogen density "at infinity" $n_0 = 0.1$ cm^{-3} and may quantatitively change for an other value of this parameter.

Acknowledgements. M.B. and D.R. thank the librarian of the Nicolas Copernicus Astronomical Center (Warsaw) for making available to them past and current issues of *Astronomy& Astrophysics* without which this research would not have been performed. The work was performed in the collaboration between the Space Research Centre of the Polish Academy of Sciences and the Institut für Astrophysik und Extraterrestrische Forschung der Universität Bonn as part of the joint project "Physics of the outer heliosphere: theory and observations" (DFG 436/POL/113/80), realised in the framework of cooperation between the Polish Academy of Sciences and Deutsche Forschungsgemeinschaft. M.B. and D.R. are grateful to the staff of the Institut für Astrophysik for the hospitality during their stay in Bonn, where the final part of the work on this paper was completed, and to the Deutsche Forschungsgemeinschaft for the financial support of this visit. The research of M.B. and D.R. presented in this paper was supported by the grant 2 P03C 013 11 from the Committee for Scientific Research (Poland).

References

Baranov V.B., Malama Yu.G., 1993, J. Geophys. Res. 98, 15157

Bertaux J.L., Lallement R., Kurt V.G., Mironova E.N., 1985, A&A 150, 1

Bzowski M., Ruciński D., 1995a, Sp. Science Rev. 72, 467

Bzowski M., Ruciński D.. 1995b, Adv. Space Res. 16 No 9, 131

Fahr H.J., 1971, A&A 14, 263

Fahr H.J., 1978, A&A 66, 103

Fahr H.J., 1979, A&A 77, 101

Fahr H.J., 1986,"The Sun and the Heliosphere in Three Dimensions", ed. R. Marsden, D. Reidel Publishing Company, 421

Fahr H.J., 1991, A&A 241, 251

Fahr H.J., 1996, Sp. Science Rev. 78, 199

Fahr H.J., Ripken H.W., 1984, A&A 139, 551

Fahr H.J., Ruciński D., Judge D.L., 1993, A&A 268, 792

Holzer T.E., 1977, Rev. Geophys. Space Phys. 15, 467

Kyrölä E., Summanen T., Råback, P., 1994, A&A 288, 299

Lallement R., 1996, Sp. Science Rev. 78, 361

Lallement R., Bertaux J.L., Kurt V.G., Mironova, E.N., 1984, A&A 140, 243

Lallement R., Bertaux J.L., Kurt V.G., 1985, J. Geophys. Res. 90, 1413

Osterbart, R., Fahr, H.J., 1992, A&A 264, 260

Pauls H.L., Zank G.P., Williams L.L., 1995, J. Geophys. Res. 100, 21595

Pauls H.L., Zank G.P., Williams L.L., 1996, "Solar Wind 8", 605

Ripken H.W., Fahr H.J., 1983, A&A 122, 181

Ruciński D., Bzowski M., 1995, A&A 296, 248

Ruciński D., Bzowski M., 1996, Sp. Science Rev. 78, 265

Scherer H., Fahr H.J., 1996, A&A, 309 957

Scherer H., Fahr H.J., 1996, Solar Physics, in press

Summanen T., 1996, A&A 314, 663

Thomas G.E., 1978, Ann. Rev. Earth Planet. Sci. 6, 173

Williams L.L., Pauls HlL., Zank G.P., 1996, "Solar Wind 8", 609

Witte M., Banaszkiewicz M., Rosenbauer H., 1996, Sp. Science Rev. 78, 289

Wu F.-M., Judge D.L., 1979, ApJ 231, 594

Wu F.-M., Judge D.L., 1980, ApJ 239, 389

Zank G.P., Pauls H.L., Williams L.C., Hall D.T., 1996, "Solar Wind 8", 654

Zank G.P., Pauls H.L., 1996, Sp. Science Rev. 78, 95

This article was processed by the author using Springer-Verlag LaTeX A&A style file *L-AA* version 3.